Journal of the Optical Society of America B
OPTICAL PHYSICS

Propagating bound states in the continuum in dielectric gratings

E. N. Bulgakov,[1,2] D. N. Maksimov,[1,2,*] P. N. Semina,[1] and S. A. Skorobogatov[1]

[1]Reshetnev Siberian State University of Science and Technology, 660037, Krasnoyarsk, Russia
[2]Kirensky Institute of Physics, Federal Research Center KSC SB RAS, 660036, Krasnoyarsk, Russia
*Corresponding author: mdn@tnp.krasn.ru

Received 8 February 2018; revised 29 March 2018; accepted 6 April 2018; posted 6 April 2018 (Doc. ID 322886); published 2 May 2018

We consider propagating bound states in the continuum in dielectric gratings. The gratings consist of a slab with ridges periodically arranged either on top or on both sides of the slab. Based on the Fourier modal approach, we recover the leaky zones above the line of light to identify the geometries of the gratings supporting Bloch bound states propagating in the direction perpendicular to the ridges. Most importantly, it is demonstrated that if a two-sided grating possesses either mirror or glide symmetry, the Bloch bound states are stable to variation of parameters as long as the above symmetries are preserved.

OCIS codes: (050.1950) Diffraction gratings; (290.4210) Multiple scattering; (350.4238) Nanophotonics and photonic crystals; (160.4236) Nanomaterials.

https://doi.org/10.1364/JOSAB.35.001218

1. INTRODUCTION

High contrast dielectric gratings (DGs) have become an important instrument in optics with various applications, including high-Q resonators and focusing reflectors [1–6]. In this paper, we address the capacity of DGs to host optical bound states in the continuum (BICs), i.e., localized eigenmodes of Maxwell's equations with infinite Q-factor embedded into the continuous spectrum of the scattering states [7]. In the recent past, the optical BICs were experimentally observed in all-dielectric setups with periodically varying permittivity [8–14]. Nowadays, the optical BICs are employed to engineer high-Q resonators for enhancement of light–matter interactions with applications to narrow-band transmission filtering [11], lasing [15], and second-harmonics generation [16].

Depending on the spacial extension of the light-holding structure, one can identify three classes of BICs. If the structure is confined in all three dimensions, a perfectly localized optical mode with infinite Q-factor can be found in spherical dielectric particles coated with zero-epsilon metamaterial [17,18]. On the other hand, if the structure is infinitely extended in one spacial dimension, the above condition on the dielectric permittivity is lifted, allowing for BICs in periodic arrays of lossless high-index dielectric elements, such as spheres [19,20] and discs [21]. Notice that in the latter case, light is localized in only two dimensions.

The third class of BIC supporting systems are planar structures infinitely extended in two dimensions. They include perforated slabs [10,22–27], arrays of rods [28–33], arrays of rectangular bars [11,13,23,25,34–37], and gratings [29,35,38–40]. Here, we consider Bloch BIC in DGs, i.e., localized modes propagating above the line of light in the plane of the structure [25,28,41–44]. Such BICs can be contrasted to symmetry-protected standing waved BICs [11,24,35,40,45] that are symmetrically mismatched with the outgoing wave allowed in the ambient medium. The Bloch BICs considered here not only provide access to light localization and concurrent effects of resonant enhancement and frequency filtering, but also allow for light guiding above the line of light paving a way for multifunction optical elements that steer the flow of light harvested from the ambient medium [46].

2. SYSTEM OVERVIEW

The simplest DG supporting BICs is sketched in Fig. 1(a). It consists of a slab substrate of thickness L made of a dielectric material with permittivity ϵ_1. Dielectric ridges of width w with permittivity ϵ_2 are placed on the top of the slab with period a in the x direction. The ridges are parallel and infinitely extended along the y axis. The whole structure is immersed into the ambient medium with $\epsilon_0 = 1$. In what follows, the thickness of the topside ridges is designated by h_1. In a more generic case of the two-sided DG shown in Fig. 1(b), the ridges are also placed on the underside of the slab. The underside ridges are positioned with the same period a to preserve the periodicity of the structure as a whole. The topside and underside ridges are shifted with respect to each other by distance δ. The thickness of the underside ridges is designated by h_2.

Due to the system's translational symmetries, the spectral parameters of the eigenmodes are linked through the following dispersion relationship [47]:

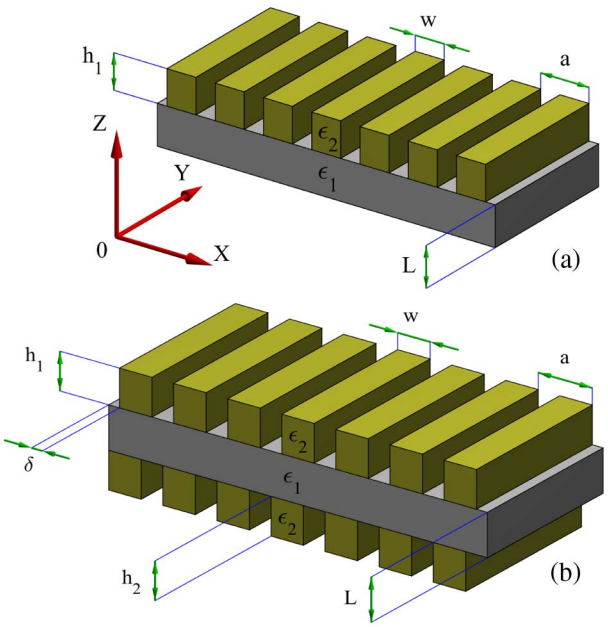

Fig. 1. Dielectric gratings: (a) one-sided grating and (b) two-sided grating.

$$k_0^2 = k_{x,n}^2 + k_z^2 + k_y^2, \qquad k_{x,n} = \beta - 2\pi n/a, \tag{1}$$

where k_0 is the vacuum wave number, $k_{x,z}$ are the wave numbers along the x, y axes, k_z is the far-field wave number in the direction orthogonal to the plane of the structure, β is the Bloch wave number, and, finally, $n = 0, 1, \ldots$ corresponds to the diffraction order. Here, we consider transverse magnetic (TM) modes with $k_y = 0$, i.e., propagating only perpendicular to the ridges; however, a generalization to bi-directional BICs propagation in both x, y directions is possible [48].

For numerical simulations, we use the rigorous Fourier modal approach in which the solution for the y component of the electric vector E_y is written in the following form [49,50]:

$$E_y(x,z) = \sum_{n=-\infty}^{\infty} S_n(z) e^{-ik_{x,n}x}. \tag{2}$$

The Fourier components $S_n(z)$ are matched on all interfaces to cast Maxwell's equations into a set of linear equations truncated in the diffraction order. Since the BICs are source-free solutions, our numerical implementation is restricted to finding the poles of the scattering matrix. All simulations are run for

$$\beta a < k_0 a < 2\pi - \beta a, \tag{3}$$

which, according to Eq. (1), means that only one TM scattering channel is open in the far-zone on both sides of the DG. We mention in passing that a similar coupled-wave approach was used in [43] for finding BICs in photonic crystal slabs with one-dimensional periodicity.

3. RESULTS

The results of our simulation for DGs with $w = 0.5a$ are collected in Table 1. Our analysis of the numerical results showed that in regard to BIC holding capacity, two major types of DGs can be distinguished. In the case of *asymmetric gratings*, the system possesses no symmetry involving mirror operation with respect to $x0y$ plane. This is always the case for the different thicknesses of the upside and underside ridges $h_1 \neq h_2$. For example, the DG shown in Fig. 1(a) clearly falls within this category. On the contrary, if $h_1 = h_2$, and $\delta = 0$, the system is mirror symmetric around its middle plane. Other types of *symmetric gratings* are those possessing a glide symmetry, i.e., a composition of a mirror reflection and a half-period translation along the x axis with $\delta = 0.5a$. In what follows, we discuss the specific features of BICs in both types of DGs.

Table 1. BICs in DG for $w = 0.5a$

BIC	$k_0 a$	βa	δ	L/a	h_1/a	h_2/a	ϵ_1	ϵ_2
1	4.829	0	0	0.1747	1	0.5	1.5	3
2	4.101	1.472	0	0.1747	1	0.5	1.5	3
3	4.168	0	N/A	0.8838	1	0	15	15
4	4.221	1.311	N/A	0.8838	1	0	15	15
5	4.168	0	0.5	0.5248	1	0.5	1.5	3
6	3.916	1.247	0.5	0.5248	1	0.5	1.5	3
7	3.644	2.001	0	1	0.5	0.5	1.5	3
8	5.094	0.690	0.5	1	0.5	0.5	1.5	3

A. Asymmetric Gratings

The BICs in asymmetric DGs are BICs 1-6 from Table 1. Among those, BICs 2,4,6 are Bloch waves with a non-zero wave vector. The mode profiles of BICs 2,4,6 are shown in Figs. 2(a)–2(c). At the same time, BICs 1,3,5 are symmetry-protected standing wave BICs previously known in literature [35,38] (not shown here for brevity). Generally, the spectrum of a DG above the line of light is characterized by leaky modes [46,51], complex eigenfrequency dispersion branches, each of which can host a BIC in an exceptional point where the eigenfrequency is real and the Q-factor diverges to infinity. In Fig. 2(d), we show the real part of the leaky-mode eigenfrequencies for three sets of the DG parameters corresponding to BICs 2,4,6. One can see that, besides a Bloch BIC, every dispersion branch also hosts a symmetry-protected standing wave BIC in the Γ-point. These standing wave BICs are BICs 1,3,5 from Table 1. The dispersion of the Q-factors is shown in Fig. 2(e) to demonstrate its divergence in the points of BICs. It is worth noting that the dispersion is symmetry with respect to $\beta \to -\beta$. Thus, each dispersion branch hosts two Bloch BICs propagating in the opposite directions.

One important feature of the asymmetric DG observed in numerical simulations is that finding a BIC always requires tuning one of the systems's parameters. For instance, in our case, the substrate thickness L always had to be adjusted to find leaky zones with a diverging Q-factor, as seen from Table 1. Given that the other parameters remain the same and the thickness is even slightly detuned from the values in Table 1, the BICs disappear from the system. That feature will be explained later in the text.

B. Symmetric Gratings

BICs 7,8 are supported by symmetric DGs. In the case of BIC 7, the DG has a mirror symmetry, while in the case of BIC 8, the DG is glide symmetric. The mode profiles of BICs 7,8 are shown in Figs. 3(a)–3(b). In contrast to asymmetric DGs, now

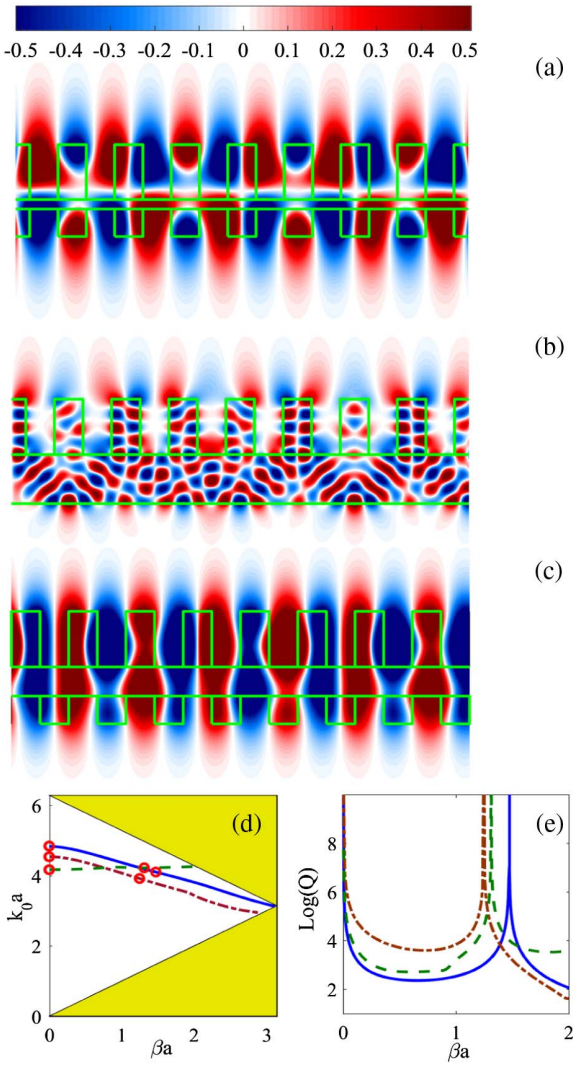

Fig. 2. BICs in asymmetric DGs. (a)–(c) Mode profiles in the form of the real part of the electric vector component E_y (p.d.u.) for BICs 2,4,6 from Table 1, respectively. (d) Dispersion of the real part of the leaky-mode frequency: BIC 2, solid blue; BIC 4, dashed green; BIC 6, dashed-dotted brown. The white domain is given by Eq. (3). Red circles show the positions of the BICs. (e) Q-factor dispersion for the same leaky zones as in (d).

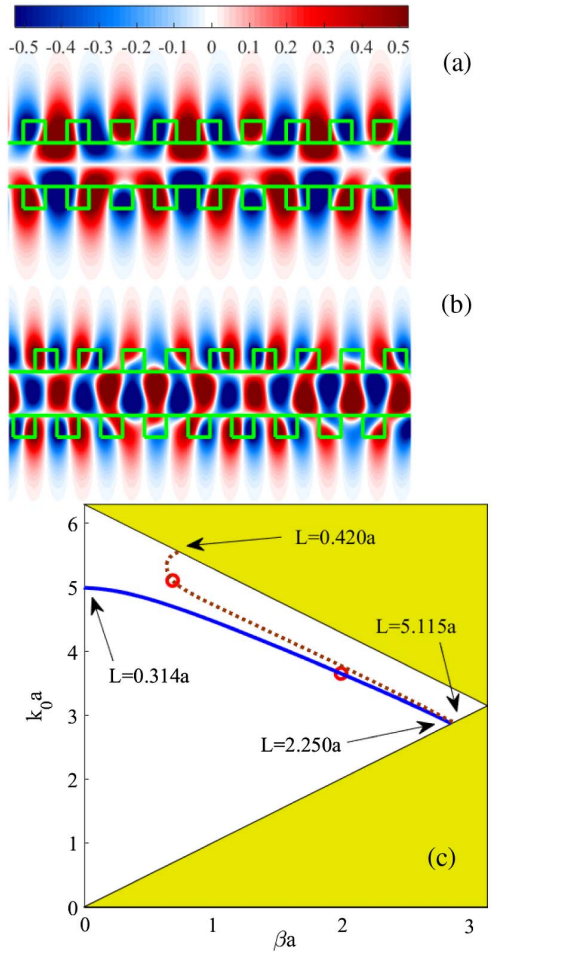

Fig. 3. BICs in symmetric DGs. (a),(b) Mode profiles in the form of the real part of the electric vector component E_y (p.d.u.) for BICs 7,8 from Table 1, respectively. (c) Position of BIC 7, solid blue, and BIC 8, dotted brown, under variation of the substrate thickness. The white domain is given by Eq. (3).

finding a BIC does not require a fine-tuning of the system's parameters. This finding complies with the results presented in [41] for double arrays of infinitely thin dielectric rods. Similar to arrays of dielectric rods [32] and perforated slabs [23], if a control parameter, such as L, is slightly perturbed, the BIC persists, having only slightly different frequency k_0 and wave vector β.

This feature can be explained in view of the topological properties of BICs in planar structures, where the BICs are known to be associated with polarization singularities (vortices) of the leaky-zone far-field polarization directions [20,23]. Since the polarization singularity is topologically stable, the variation of parameters relocates only the position of polarization vortex in momentum space. Once the DG is symmetric, the leaky modes also possess identical far-field patterns in upper and lower half-spaces that can be shifted only with respect to each other in the case of the glide symmetry. Therefore, under variation of parameters, the polarization vortex migrates in the same point in both upper and lower half-spaces, ensuring the stability of the BIC. This, however, is not the case for asymmetric DG when the BIC field pattern is also asymmetric. Once the control parameter is perturbed, the polarization vortices are relocated in momentum-space in both upside and underside far-field polarization patterns. Although the polarization vortices persist, due to the absence of symmetry, their positions do not have to coincide. Thus, Bloch BICs in asymmetric DGs are purely accidental in nature, which explains their fragility to variation of parameters.

Finally, let us illustrate the above arguments with numerical data. In Fig. 3(c), we show the frequencies of the families of BICs generated by BIC 7 and 8 under variation of the substrate thickness L. It is seen from Fig. 3(c) that with an increase of L, both BICs shift to the line of light $k_0 = \beta$ until they eventually

cross it to become ordinary guided modes below the line of light protected by total internal reflection. With the decrease of L, the scenarios are, however, different. The family generated by BIC 8 terminates at the line $k_0 a = 2\pi - \beta a$, which is the boundary of the second radiation continuum. Once that boundary is crossed, the BIC is destroyed by leakage to the second radiation channel. In contrast to the above case, BIC 7 migrates to the Γ-point, where all three BICs, i.e., one symmetry protected and two Bloch waves propagating in the opposite directions, hosted by the leaky zone coalesce. In this point, the Bloch BICs vanish, transforming to BICs propagating along the y axis to which they are continuously connected across the gamma point (see [20] for more detail).

4. CONCLUSION

We considered Bloch bound states in the continuum in DGs. Based on the Fourier modal approach, we recovered the leaky zones above the line of light to identify the geometries of the gratings supporting Bloch bound states propagating in the direction perpendicular to the ridges. It is shown that the capacity of DGs to host such bound states depends on the presence/absence of symmetry with respect to the central plane of the grating. It is demonstrated that if a two-sided grating possesses either mirror or glide symmetry, the Bloch bound states are stable to variation of parameters, as long as the above symmetries are preserved. That makes the bound states robust against possible fabrication inaccuracies and at the same time allowing for a certain freedom in choosing the geometric parameters of the gratings. We speculate that our finding might be useful in design of multifunction optical elements that steer the flow of light harvested from the ambient medium.

Funding. Ministry of Education and Science of the Russian Federation (Minobrnauka) (State Contract No 3.1845.2017/4.6).

REFERENCES

1. Y. Zhou, M. Moewe, J. Kern, M. C. Huang, and C. J. Chang-Hasnain, "Surface-normal emission of a high-"q" resonator using a subwavelength high-contrast grating," Opt. Express **16**, 17282–17287 (2008).
2. D. Fattal, J. Li, Z. Peng, M. Fiorentino, and R. G. Beausoleil, "Flat dielectric grating reflectors with focusing abilities," Nat. Photonics **4**, 466–470 (2010).
3. F. Lu, F. G. Sedgwick, V. Karagodsky, C. Chase, and C. J. Chang-Hasnain, "Planar high-numerical-aperture low-loss focusing reflectors and lenses using subwavelength high contrast gratings," Opt. Express **18**, 12606–12614 (2010).
4. V. Karagodsky, C. Chase, and C. J. Chang-Hasnain, "Matrix Fabry–Perot resonance mechanism in high-contrast gratings," Opt. Lett. **36**, 1704–1706 (2011).
5. C. J. Chang-Hasnain and W. Yang, "High-contrast gratings for integrated optoelectronics," Adv. Opt. Photon. **4**, 379–440 (2012).
6. Y. H. Ko, M. Niraula, K. J. Lee, and R. Magnusson, "Properties of wideband resonant reflectors under fully conical light incidence," Opt. Express **24**, 4542–4551 (2016).
7. C. W. Hsu, B. Zhen, A. D. Stone, J. D. Joannopoulos, and M. Soljačić, "Bound states in the continuum," Nat. Rev. Mater. **1**, 16048 (2016).
8. Y. Plotnik, O. Peleg, F. Dreisow, M. Heinrich, S. Nolte, A. Szameit, and M. Segev, "Experimental observation of optical bound states in the continuum," Phys. Rev. Lett. **107**, 28–31 (2011).
9. S. Weimann, Y. Xu, R. Keil, A. E. Miroshnichenko, A. Tünnermann, S. Nolte, A. A. Sukhorukov, A. Szameit, and Y. S. Kivshar, "Compact surface fano states embedded in the continuum of waveguide arrays," Phys. Rev. Lett. **111**, 240403 (2013).
10. C. W. Hsu, B. Zhen, J. Lee, S.-L. Chua, S. G. Johnson, J. D. Joannopoulos, and M. Soljačić, "Observation of trapped light within the radiation continuum," Nature **499**, 188–191 (2013).
11. J. M. Foley, S. M. Young, and J. D. Phillips, "Symmetry-protected mode coupling near normal incidence for narrow-band transmission filtering in a dielectric grating," Phys. Rev. B **89**, 165111 (2014).
12. R. A. Vicencio, C. Cantillano, L. Morales-Inostroza, B. Real, C. Meja-Cortés, S. Weimann, A. Szameit, and M. I. Molina, "Observation of localized states in Lieb photonic lattices," Phys. Rev. Lett. **114**, 245503 (2015).
13. Z. F. Sadrieva, I. S. Sinev, K. L. Koshelev, A. Samusev, I. V. Iorsh, O. Takayama, R. Malureanu, A. A. Bogdanov, and A. V. Lavrinenko, "Transition from optical bound states in the continuum to leaky resonances: role of substrate and roughness," ACS Photon. **4**, 723–727 (2017).
14. Y.-X. Xiao, G. Ma, Z.-Q. Zhang, and C. Chan, "Topological subspace-induced bound state in the continuum," Phys. Rev. Lett. **118**, 166803 (2017).
15. A. Kodigala, T. Lepetit, Q. Gu, B. Bahari, Y. Fainman, and B. Kanté, "Lasing action from photonic bound states in continuum," Nature **541**, 196–199 (2017).
16. T. Wang and S. Zhang, "Large enhancement of second harmonic generation from transition-metal dichalcogenide monolayer on grating near bound states in the continuum," Opt. Express **26**, 322–337 (2018).
17. F. Monticone and A. Alù, "Embedded photonic eigenvalues in 3D nanostructures," Phys. Rev. Lett. **112**, 213903 (2014).
18. J. Li, J. Ren, and X. Zhang, "Three-dimensional vector wave bound states in a continuum," J. Opt. Soc. Am. B **34**, 559–565 (2017).
19. E. N. Bulgakov and A. F. Sadreev, "Light trapping above the light cone in a one-dimensional array of dielectric spheres," Phys. Rev. A **92**, 023816 (2015).
20. E. N. Bulgakov and D. N. Maksimov, "Topological bound states in the continuum in arrays of dielectric spheres," Phys. Rev. Lett. **118**, 267401 (2017).
21. E. N. Bulgakov and A. F. Sadreev, "Bound states in the continuum with high orbital angular momentum in a dielectric rod with periodically modulated permittivity," Phys. Rev. A **96**, 013841 (2017).
22. S. P. Shipman and S. Venakides, "Resonant transmission near nonrobust periodic slab modes," Phys. Rev. E **71**, 026611 (2005).
23. B. Zhen, C. W. Hsu, L. Lu, A. D. Stone, and M. Soljačić, "Topological nature of optical bound states in the continuum," Phys. Rev. Lett. **113**, 257401 (2014).
24. V. Mocella and S. Romano, "Giant field enhancement in photonic resonant lattices," Phys. Rev. B **92**, 155117 (2015).
25. L. Ni, Z. Wang, C. Peng, and Z. Li, "Tunable optical bound states in the continuum beyond in-plane symmetry protection," Phys. Rev. B **94**, 245148 (2016).
26. L. Li and H. Yin, "Bound states in the continuum in double layer structures," Sci. Rep. **6**, 26988 (2016).
27. E. Penzo, S. Romano, Y. Wang, S. Dhuey, L. D. Negro, V. Mocella, and S. Cabrini, "Patterning of electrically tunable light-emitting photonic structures demonstrating bound states in the continuum," J. Vac. Sci. Technol. B **35**, 06G401 (2017).
28. S. Venakides and S. P. Shipman, "Resonance and bound states in photonic crystal slabs," SIAM J. Appl. Math. **64**, 322–342 (2003).
29. D. C. Marinica, A. G. Borisov, and S. V. Shabanov, "Bound states in the continuum in photonics," Phys. Rev. Lett. **100**, 183902 (2008).
30. E. N. Bulgakov and A. F. Sadreev, "Bloch bound states in the radiation continuum in a periodic array of dielectric rods," Phys. Rev. A **90**, 053801 (2014).
31. L. Yuan and Y. Y. Lu, "Propagating Bloch modes above the lightline on a periodic array of cylinders," J. Phys. B **50**, 05LT01 (2017).
32. L. Yuan and Y. Y. Lu, "Bound states in the continuum on periodic structures: perturbation theory and robustness," Opt. Lett. **42**, 4490–4493 (2017).

33. Z. Hu and Y. Y. Lu, "Resonances and bound states in the continuum on periodic arrays of slightly noncircular cylinders," J. Phys. B **51**, 035402 (2018).
34. C. Blanchard, J.-P. Hugonin, and C. Sauvan, "Fano resonances in photonic crystal slabs near optical bound states in the continuum," Phys. Rev. B **94**, 155303 (2016).
35. X. Cui, H. Tian, Y. Du, G. Shi, and Z. Zhou, "Normal incidence filters using symmetry-protected modes in dielectric subwavelength gratings," Sci. Rep. **6**, 36066 (2016).
36. Z. Wang, H. Zhang, L. Ni, W. Hu, and C. Peng, "Analytical perspective of interfering resonances in high-index-contrast periodic photonic structures," IEEE J. Quantum Electron. **52**, 1–9 (2016).
37. A. Taghizadeh and I.-S. Chung, "Quasi bound states in the continuum with few unit cells of photonic crystal slab," Appl. Phys. Lett. **111**, 031114 (2017).
38. J. W. Yoon, S. H. Song, and R. Magnusson, "Critical field enhancement of asymptotic optical bound states in the continuum," Sci. Rep. **5**, 18301 (2015).
39. F. Monticone and A. Alù, "Bound states within the radiation continuum in diffraction gratings and the role of leaky modes," New J. Phys. **19**, 093011 (2017).
40. Y. Wang, J. Song, L. Dong, and M. Lu, "Optical bound states in slotted high-contrast gratings," J. Opt. Soc. Am. B **33**, 2472–2479 (2016).
41. R. F. Ndangali and S. V. Shabanov, "Electromagnetic bound states in the radiation continuum for periodic double arrays of subwavelength dielectric cylinders," J. Math. Phys. **51**, 102901 (2010).
42. Y. Yang, C. Peng, Y. Liang, Z. Li, and S. Noda, "Analytical perspective for bound states in the continuum in photonic crystal slabs," Phys. Rev. Lett. **113**, 037401 (2014).
43. X. Gao, C. W. Hsu, B. Zhen, X. Lin, J. D. Joannopoulos, M. Soljačić, and H. Chen, "Formation mechanism of guided resonances and bound states in the continuum in photonic crystal slabs," Sci. Rep. **6**, 31908 (2016).
44. Z. Hu and Y. Y. Lu, "Propagating bound states in the continuum at the surface of a photonic crystal," J. Opt. Soc. Am. B **34**, 1878–1883 (2017).
45. V. Pacradouni, W. J. Mandeville, A. R. Cowan, P. Paddon, J. F. Young, and S. R. Johnson, "Photonic band structure of dielectric membranes periodically textured in two dimensions," Phys. Rev.B **62**, 4204–4207 (2000).
46. E. N. Bulgakov and D. N. Maksimov, "Light guiding above the light line in arrays of dielectric nanospheres," Opt. Lett. **41**, 3888–3891 (2016).
47. E. Popov, *Gratings: Theory and Numeric Applications* (Institut Fresnel, 2012).
48. E. N. Bulgakov and D. N. Maksimov, "Bound states in the continuum and polarization singularities in periodic arrays of dielectric rods," Phys. Rev. A **96**, 063833 (2017).
49. M. Pisarenco, J. Maubach, I. Setija, and R. Mattheij, "Aperiodic fourier modal method in contrast-field formulation for simulation of scattering from finite structures," J. Opt. Soc. Am. A **27**, 2423–2431 (2010).
50. M. Pisarenco, J. Maubach, I. Setija, and R. Mattheij, "Modified s-matrix algorithm for the aperiodic Fourier modal method in contrast-field formulation," J. Opt. Soc. Am. A **28**, 1364–1371 (2011).
51. F. Monticone and A. Alu, "Leaky-wave theory, techniques, and applications: from microwaves to visible frequencies," Proc. IEEE **103**, 793–821 (2015).